Atmos. Chem. Phys. Discuss., 12, 4447–4476, 2012
www.atmos-chem-phys-discuss.net/12/4447/2012/
doi:10.5194/acpd-12-4447-2012

Atmospheric Chemistry and Physics Discussions

Humidity-dependent phase state of SOA particles from biogenic and anthropogenic precursors

E. Saukko[1], A. T. Lambe[2,3], P. Massoli[3], Koop, T. [4], J. P. Wright[2], D. R. Croasdale[2], D. A. Pedernera[4,*], T. B. Onasch[2,3], A. Laaksonen[5,6], P. Davidovits[2], D. R. Worsnop[3,7], and A. Virtanen[1,]**

[1]Department of Physics, Tampere University of Technology, Tampere, Finland
[2]Chemistry Department, Boston College, Chestnut Hill, MA, USA
[3]Aerodyne Research Inc., Billerica, MA, USA
[4]Faculty of Chemistry, Bielefeld University, Bielefeld, Germany
[5]Finnish Meteorological Institute, Helsinki, Finland
[6]Department of Applied Physics, University of Eastern Finland, Kuopio, Finland
[7]Division of Atmospheric Sciences, Department of Physics, University of Helsinki, Helsinki, Finland
[*]now at: Faculty of Mathematics, Astronomy and Physics, National University of Córdoba, Córdoba, Argentina

**now at: Department of Applied Physics, University of Eastern Finland, Kuopio, Finland

Received: 22 December 2011 – Accepted: 28 January 2012 – Published: 8 February 2012

Correspondence to: A. Virtanen (annele.virtanen@uef.fi)

Published by Copernicus Publications on behalf of the European Geosciences Union.

Abstract

The physical phase state (solid, semi-solid, or liquid) of secondary organic aerosol (SOA) particles has important implications for a number of atmospheric processes. We report the phase state of SOA particles spanning a wide range of oxygen to carbon ratios (O/C), used here as a surrogate for SOA oxidation level, produced in a flow tube reactor by photo-oxidation of various atmospherically relevant surrogate anthropogenic and biogenic volatile organic compounds (VOCs). The phase state of laboratory-generated SOA was determined by the particle bounce behavior after inertial impaction on a polished steel substrate. The measured bounce fraction was evaluated as a function of relative humidity and SOA oxidation level (O/C) measured by an Aerodyne high resolution time of flight aerosol mass spectrometer (HR-ToF AMS).

The main findings of the study are: (1) Biogenic and anthropogenic SOA particles are found to be solid or semi-solid until a relative humidity of at least 50 % RH at impaction is reached. (2) Long-chain alkanes produce liquid SOA particles when generated at low oxidation level of O/C<0.2, but at higher oxidation levels they solidify. (3) Increasing sulphuric acid (H_2SO_4) within the SOA particles reduces the threshold of humidity-induced phase changes. (4) The bounce behavior of the various SOA systems did not show a consistent linear relationship with the particle O/C. Rather, the molar mass of the gas-phase VOC precursor showed a positive correlation with the resistance to the RH-induced phase change of the formed SOA particles.

1 Introduction

The direct and indirect effects of aerosol particles on the Earth's radiative budget remain the largest source of uncertainty in climate change modeling (IPCC, 2007, ch.2). Organic matter (OM) forms up to 90 % of observed aerosol particulate mass, and secondary organic aerosol (SOA) represents up to half of the organic fraction (Jimenez et al., 2009; Hallquist et al., 2009) on the global scale. SOA particles are generally

ACPD
12, 4447–4476, 2012

associated with a direct cooling effect as they scatter the incoming solar light and they participate in cloud formation by acting as cloud condensation nuclei, CCN (IPCC, 2007, ch.2).

SOA particles are formed from oxidation of gas-phase organic precursors. The volatility of the VOCs decreases as their functionalization and thus binding ability increases (Donahue et al., 2012), causing their vapor pressure to decrease until the gaseous compounds either condense on existing particles or nucleate to form new particles. The SOA formation process under natural conditions is complicated and it involves a multitude of gaseous precursors and significantly greater number of particle product compounds. Up to now, the modeling of formation and aging of SOA has been mostly based on gas-particle equilibrium partitioning of volatile and semivolatile species (Pankow, 1994; Kanakidou et al., 2005). This implies fast enough condensed phase diffusion rates to keep the condensed phase in equilibrium with the gas phase as the particles' size increases and the concentration of VOCs decreases.

However, several recent studies show that at least under some conditions natural and laboratory-produced SOA particles have an amorphous solid state (Virtanen et al., 2010; Cappa and Wilson, 2011; Vaden et al., 2011). The solid amorphous state of SOA particles has important implications for a number of atmospheric processes. First, a solid phase implies surface-confined chemistry and kinetic limitations to achieve equilibrium partitioning between the gas phase and the particle phase. More importantly, chemical reactions are impeded in viscous aerosol particles (Zahardis and Petrucci, 2007; Shiraiwa et al., 2011; Pfrang et al., 2011), because mass transport (diffusion) of reactants within the aerosol particle bulk may become the rate limiting step. Shiraiwa et al. (2011) showed that these kinetic limitations can increase the chemical lifetime of (semi-)solid particles by more than an order of magnitude. The water uptake of highly viscous SOA particles may also be diminished or even fully inhibited, in particular at low temperatures, with implications for the particles' size and scattering properties and their direct effect on climate (Zobrist et al., 2008; Murray, 2008; Mikhailov et al., 2009; Koop et al., 2011).

ACPD
12, 4447–4476, 2012

All recent studies reporting a solid phase of SOA particles (Virtanen et al., 2010; Cappa and Wilson, 2011; Vaden et al., 2011) have focused on studying the properties of SOA produced from oxidation products of α-pinene or of SOA produced from VOCs emitted by pine trees and measured under dry conditions (RH<40%). In order to assess how general is the occurence of the amorphous solid state of the SOA, and how other factors might affect particle phase state, we report a systematic characterization of laboratory SOA generated from the OH oxidation of several atmospherically relevant anthropogenic and biogenic precursors as a function of hydroxyl radical (*OH) exposure and relative humidity.

2 Experimental

The general experimental procedure was to produce a stable SOA population selected with respect to particle number and mass-weighted size distributions and chemical composition. The SOA particles were subsequently characterized with an instrument array consisting of a Scanning Mobility Particle Sizer (SMPS) (TSI), Cloud Condensation Nuclei Counter (CCNC) (CCNC-100, Droplet Measurement Technologies), High-Resolution Time-of-Flight Aerosol Mass Spectrometer (HR-ToF-AMS) (Aerodyne) and a low pressure impactor (LPI) equipped with an optical counting arrangement.

The LPI technique, which is described in more detail in Sect. 2.2, provides a measurement of the phase of the SOA particles. Liquid particles are collected on the impactor stage with minimal bounce, whereas solid SOA particles are likely to bounce upon striking the surface of the impactor stage.

In this work, the number concentration of the sampled SOA particles is measured upstream and downstream of the impactor. Detection of particles downstream of the impactor indicates that particles are bouncing off of the impactor stage and suggests the presence of an amorphous semi-solid or solid state.

ACPD
12, 4447–4476, 2012

2.1 SOA particle generation

SOA particles were generated with a Potential Aerosol Mass (PAM) flow tube reactor. The reactor is capable of simulating atmospheric oxidation timescales of days to weeks with actual residence times of minutes. The details of the reactor used are described in Lambe et al. (2011).

SOA precursors were oxidized in a PAM flow reactor, which is a horizontal 15 l glass cylindrical chamber 46 cm long ×22 cm ID. Organic species were transported through the PAM reactor by a carrier gas consisting of 8.5 lpm N_2 and 0.5 lpm O_2. The average species residence time in the PAM reactor was typically 100 s. Four mercury lamps (BHK Inc.) with peak emission intensity at $\lambda = 254$ nm were mounted in teflon-coated quartz cylindrical sleeves inside the chamber, and were continually purged with N_2.

OH radicals (*OH) were produced via the reaction $O_3 + h\nu \rightarrow O_2 + O(^1D)$ followed by the reaction $O(^1D) + H_2O \rightarrow 2\,^*OH$. O_3 was generated by irradiating O_2 with a mercury lamp ($\lambda = 185$ nm) outside the PAM reactor. Oxygen ($O(^1D)$) radicals were produced by UV photolysis of O_3 inside the PAM reactor. The radical $O(^1D)$ then reacted with water vapor (introduced using a heated Nafion membrane humidifier; Perma Pure LLC) to produce OH radicals inside the PAM reactor. Most experiments were conducted at relative humidities ranging from 30 % to 40 %, depending on the temperature in the PAM reactor (22–32 °C) at different UV lamp settings. At a given measured relative humidity, this parameter remained constant to within ±5 %. We note that the relative humidity in the PAM is distinct from the relative humidity in the low pressure impactor, which is discussed in the next section.

The *OH exposure, which is the product of the OH concentration and the average residence time in the PAM reactor, was varied by changing the UV light intensity through stepping the voltage applied to the lamps between 0 and 110 V. The *OH exposure was determined indirectly by measuring the decay of SO_2 due to reaction with OH in the PAM reactor. SO_2 calibration measurements were conducted as a function of UV lamp intensity and O_3 concentration (Lambe et al., 2011). Typical *OH exposures

ACPD
12, 4447–4476, 2012

ranged from 2.7×10^{11} to 2.2×10^{12} molec cm^{-3} s. These values are equivalent to 2 to 17 days of atmospheric oxidation assuming an average atmospheric *OH concentration of 1.5×10^{6} molec cm^{-3} (Mao et al., 2009). While O_3 and *OH can oxidize organic species, *OH was the principal oxidant in all experiments except for selected studies, where experiments with O_3 as the oxidizing agent were conducted by turning the lamps off. Prior to each experiment, the PAM reactor was conditioned with *OH radicals until a particle background less than 10 particles cm^{-3} was attained.

In some experiments, internally mixed SOA – sulfuric acid particles were produced by introducing SO_2 along with the SOA precursor, which is oxidized by *OH to produce sulfuric acid (H_2SO_4) in the presence of water vapor (Seinfeld and Pandis, 1998, ch. 6.13).

Gas-phase SOA precursors used in these experiments were α-pinene, longifolene, isoprene, naphthalene and *n*-heptadecane. SOA was generated via gas-phase oxidation of precursors, followed by homogeneous nucleation. Volatile organic compound (VOC) precursors used in this study were isoprene and α-pinene. VOC precursors were prepared in compressed gas cylinders or in glass bubblers and introduced into the PAM reactor with N_2 carrier gas at controlled rates using a mass-flow controller. Intermediate volatility organic compound (IVOC) precursors used in this study were *n*-heptadecane, longifolene, and naphthalene. With the exception of naphthalene, IVOCs were introduced into the carrier gas flow using a permeation tube placed in a temperature-controlled oven. Naphthalene vapor was introduced by flowing N_2 over solid naphthalene placed in a Teflon tube.

2.2 SOA particle bounce measurement

The low pressure impactor used in this study to measure the particle bounce is described in detail in Saukko et al. (2012). Briefly, the core system consists of a low pressure impactor and a polished steel substrate that minimizes the surface area and impacts with a glancing angle. Size-selected aerosol is guided through a sampling cell

ACPD
12, 4447–4476, 2012

(see Fig. 2) at low pressure until the system is stabilized, after which the cell is closed and re-pressurised to bring the sample to working conditions of a TSI Ultrafine Water Condensation Particle Counter (WCPC). This particle number concentration is compared to the particle concentration measured upstream of the impactor. The *bounced fraction* is the ratio of concentrations after and before the impactor, divided by the same ratio with a baseline sample without the impaction substrate. The particles with high bounced fraction are more solid than those with low bounced fraction. Accurate scales relating the bounced fraction to mechanical or other properties of the particles have not, however, been established yet. The bounced fraction for dry ammonium sulfate particles is around 0.8 and it is 0 when they are deliquesced (Saukko et al., 2012). The particle sizes used in the experiments were between 105 and 160 nm in mobility diameter, and 130 to 230 nm in aerodynamic diameter.

The humidity of the sampled aerosol is adjusted between 28 and 91 % RH by a Nafion humidifier (PermaPure). The Nafion capillaries are fed with a mixture of ~100 % RH air from water-fed micro-pore humidifier (Enerfuel) and <5% RH pressurized air. The aerosol sample flows around the Nafion capillaries and the water vapor is transferred from the humidifying flow. The output humidity is adjusted with the ratio of the saturated and <5% RH airflows.

The relative humidity history of the sampled aerosol is slightly more complicated than the simple humidification by the Nafion tube: as the aerosol enters the impactor, the upstage pressure is 690 kPa, which is approximately 70 % of the ambient pressure. Thus, the water vapour is diluted by expansion and the range of sample relative humidities upstream of the impactor (28 % to 91 % RH) corresponds to a range of reduced relative humidities of 20 % to 64 % RH inside the impactor. The equilibration time for the aerosol at this reduced RH is about 0.9 s (Saukko et al., 2012), which at room temperature is sufficient for ~100 nm particles to equilibrate with the gas phase humidity even if a semi-solid or solid state was obtained prior to entering the impactor (Koop et al., 2011; Zobrist et al., 2011).

ACPD
12, 4447–4476, 2012

2.3 SOA CCN activity

The CCN activity of SOA particles was measured with a continuous flow CCN counter (CCNC) (Roberts and Nenes, 2005; Lance et al., 2006). The PAM-generated SOA was size-selected using a TSI 3080 DMA prior to CCN number concentration measurements with the CCNC and total particle number concentration measurements with a CPC (TSI 3022A). CCN activation curves were generated by holding the particle size constant while systematically varying the CCNC column temperature gradient to obtain controlled water vapor supersaturation between 0.1–1.5 % or until 100 % activation was reached, as described in Massoli et al. (2010) and Lambe et al. (2011). The CCN activity, κ, was calculated using the approach by Petters and Kreidenweis (2007). Selected dry mobility diameters ranged from 55 to 85 nm for SOA.

2.4 SOA mass spectra and elemental ratios

Mass spectra of the aerosol were obtained with an Aerodyne HR-ToF-AMS (DeCarlo et al., 2006). Elemental analysis yielding oxygen-to-carbon (O/C) and hydrogen-to-carbon (H/C) ratios was performed on high-resolution ToF-AMS (HR-ToF-AMS) measurements using ToF-AMS analysis software (Squirrel and Pika: http://cires.colorado.edu/jimenez-group/ToFAMSResources/ToFSoftware/index.html). (Aiken et al., 2008)

3 Results and discussion

Table 1 shows the range of O/C ratio (0.10 to 1.41), H/C ratio (1.92 to 0.90) and CCN κ-values (0.01 to 0.20) for the SOA particles that were studied in this work, along with the corresponding *OH exposures in the PAM reactor.

ACPD
12, 4447–4476, 2012

3.1 Phase state and humidity-induced phase transitions of biogenic SOA particles

The fraction of bounced SOA particles formed from biogenic precursors (isoprene, α-pinene, and longifolene) was characterized as a function of relative humidity in the impactor. As mentioned in Sect. 2.2, the relative humidity in the impactor is 70 % of the initial sample relative humidity. We denote the RH value inside the impactor the impactor RH, RH_I.

For 20 % $<RH_I<$50 %, the bounced fraction of biogenic SOA particles was approximately 0.8 in all cases (Fig. 3; solid lines are fits to guide the eye). The measured bounced fraction of dry ammonium sulphate particles sampled with the impactor is also approximately 0.8 (rather than 1) as discussed in Sect. 2.2. Thus, we conclude that biogenic SOA particles generated in the PAM reactor are solid or semi-solid at $RH_I<50$ % over the range of measured conditions.

For 50 %$<RH_I<$64 %, the measured bounced fraction of biogenic SOA particles decreased. The decrease in bounced fraction was most pronounced for SOA particles generated from isoprene, where the bounced fraction decreased to approximately 0.1 at $RH_I = 65$ % (Fig. 3, top panel). This decrease in bounce suggests a decrease in viscosity as a result of a humidity-induced phase change from solid to liquid-like particles.

Similar measurements of bounced fraction as a function of RH_I were performed for SOA particles generated from α-pinene (Fig. 3 middle panel) and longifolene (Fig. 3 lower panel). The middle panel also shows that there was no systematic difference in the measured bounced fraction for α-pinene SOA particles as a function of O/C ratio (O/C = 0.34 to 0.69). For SOA particles generated from α-pinene, the bounced fraction decreased from approximately 0.8 to 0.5 as a function of RH_I. This decrease in bounce was significantly less than for SOA produced from isoprene, suggesting that phase changes were less pronounced.

For SOA particles generated from longifolene, the bounced fraction decreased from approximately 0.8 to 0.7 as a function of RH_I. There was no noticeable change in

ACPD
12, 4447–4476, 2012

bounced fraction as a function of O/C ratio, which ranged from 0.14 to 0.58 for longifolene SOA. Thus, for SOA generated from the three biogenic precursors that were studied in this work, the RH_l-dependent decrease in bounced fraction became less pronounced with increasing molar mass of the precursor. If we assume that the molar mass of the precursor is proportional to the average molecular mass (AMM) of the SOA generated from that precursor, this suggests that changes in the measured bounced fraction are higher for SOA with smaller AMM and lower for SOA with larger AMM. This behavior is in accordance with the fact that molecular compounds with larger molar mass show a higher glass transition temperature T_g than those with smaller molar mass (Koop et al., 2011). A higher T_g usually implies that a larger water content (and, hence, higher RH_l) is required to liquefy a particle, see below.

3.2 Phase state and humidity-induced phase transitions of mixed SOA-sulphuric acid particles

In most cases, ambient oxygenated organic aerosol (OOA) is mixed with inorganic species such as particulate nitrate and sulphate, (e.g., (Jimenez et al., 2009)), which may influence the viscosity or phase of the aerosols. In a separate set of experiments, we measured the bounced fraction of SOA/sulphuric acid mixtures generated from the simultaneous oxidation of longifolene and SO_2 in the PAM reactor. This combination of precursors simplifies interpretation of the data because the bounced fraction of longifolene SOA (0.7–0.8) is insensitive to RH_l. Therefore, any changes in particle bounce are due to changes in the organics-to-sulphate ratio of the particles (measured by the AMS). AMS particle time-of-flight measurements confirmed that the SOA and sulphuric acid were internally mixed in all cases.

Figure 4 shows the measured bounced fraction as a function of RH_l for SOA-sulphuric acid mixtures, with sulphate mass fractions ranging from 0.09 to 0.36. The sulfate fraction is the mass fraction of sulfate compared to the total mass of particles composed of organic carbon compounds, sulfate and ammonia. The ammonia is presumably from trace concentrations from the PAM system and makes up 11–14 % of the total mass.

ACPD
12, 4447–4476, 2012

As is evident from Fig. 4, a sulphate mass fraction of 0.09 does not decrease the particle bounce relative to that of pure longifolene SOA. However, increasing the sulphate mass fraction to 0.20 results in a continual decrease in particle bounced fraction as a function of RH_l, with the sharpest decrease at RH_l ~55 %, to a final bounced fraction less than 0.1 at RH_l = 62 %. This suggests a solid-to-liquid phase transition of the mixed SOA/sulfate particles in this range of RH_l. Increasing the sulphate mass fraction to 0.36 results in a constant particle bounced fraction ¡ 0.10 for 20 %¡RH_l<62 %, implying a liquid state over the entire RH_l range investigated.

The behavior of mixed organic/sulphate particles was further examined using differential scanning calorimetry (DSC) (Höhne et al., 2003) to measure the glass transition temperature (T_g) of model mixtures of glucose and sulphuric acid, for experimental details see Zobrist et al. (2008). Figure 5 shows that increasing the mass fraction of sulphuric acid decreases the glass transition temperature of the mixture at constant solute mass fraction (i.e., constant water content). Our results are therefore consistent with studies showing that mixing compounds with different T_g values normally results in a glass transition temperature of the mixture that is between T_g values of the individual mixture components (Zobrist et al., 2008; Koop et al., 2011).

Accordingly, because sulphuric acid shows a lower T_g than the organics investigated here, its presence softens the SOA particles. Moreover, owing to its larger hygroscopicity sulphuric acid (and similarly ammonium bisulfate or ammonium sulfate) also leads to an increase in water content of the particles at the same RH, further softening the particles, thereby leading to a humidity-induced liquefaction of the particles at lower humidities when compared to pure SOA particles. This is shown schematically in the bottom panel of Fig. 5, which is a sketch of T_g versus equilibrium relative humidity for various organics and/or sulphuric acid mixtures. When humidity is increased at constant temperature (black arrow) the pure organic (green curve) with the highest glass transition temperature in the dry state, $T_g(dry)$, shows a humidity-induced liquefaction at the highest RH (intersection between the black arrow and the green T_g curve), close to the upper end of investigated RH range.

ACPD
12, 4447–4476, 2012

In contrast, pure sulphuric acid or a mixture with high sulphuric acid content (red) show the lowest T_g(dry) and, hence, are liquid over the full range of investigated RH without any bounce. Finally, a mixture with a high organics content (orange) shows an intermediate T_g(dry), thus liquefying at an intermediate RH in the middle of the investigated RH range.

We conclude, that if sulphuric acid plays an important role in atmospheric nucleation processes, as suggested by Sipilä et al. (2010) and Kirkby et al. (2011), our results suggest that freshly nucleated particles containing appreciable amounts of sulphuric acid are initially liquid. As the particles grow via condensation of oxygenated organic species, the mass fraction and, hence, the effective T_g increases and the particles may solidify (Virtanen et al., 2010, 2011).

3.3 Phase state and humidity-induced phase transitions of anthropogenic SOA particles

In addition to bounce measurements of biogenic SOA particles, we also studied the bounce behavior of anthropogenic SOA particles generated from the oxidation of naphthalene and *n*-heptadecane. Naphthalene was chosen as a model aromatic precursor, and *n*-heptadecane as a model aliphatic precursor. The upper panel in Fig. 6 shows the bounced fraction of SOA particles generated from naphthalene as a function of RH_l. The bounce behavior for naphthalene SOA is similar to that of α-pinene SOA, with a decrease in bounced fraction from 0.6–0.7 at RH_l<50 % to 0.3–0.5 at RH_l = 64 %.

The lower panel in Fig. 6 shows the bounce behavior of *n*-heptadecane SOA as a function of RH_l. The figure indicates that, unlike the other systems that were studied, the bounced fraction of SOA particles generated from *n*-heptadecane was strongly correlated with the O/C ratio of the SOA. At O/C = 0.10, the SOA bounced fraction was low (0.2) and was unaffected by RH_l, implying an organic liquid-like phase. At O/C = 0.15, the bounced fraction was about 0.5 at RH_l = 20 % and exhibited a monotonic decrease to 0.2 at RH_l = 64 %. At O/C = 0.21, a constant bounced fraction of 0.6 was measured for RH_l<50 %, with a decrease in bounced fraction to 0.4 at RH_l = 64 %. This bounce

ACPD
12, 4447–4476, 2012

behavior is consistent with a semi-solid particle phase. Finally, at an O/C ratio of 0.30, we measured a constant bounced fraction of 0.8 at RH_l<50 % before the bounced fraction decreased to 0.6 at RH_l = 64 %. This bounce behavior was similar to that observed in the other systems that were studied. Thus, SOA particles generated from *n*-heptadecane were initially liquid-like at low O/C ratio and solidified with increasing O/C ratio.

In order to rationalize the observed behavior of the anthropogenic SOA particles we show in Fig. 7 predicted T_g values for naphthalene (~247 K) and *n*-heptadecane (~207 K). These T_g values were predicted from the observed dependence of T_g upon melting temperature T_m, i.e. $T_g \approx 0.7 \times T_m$ (Koop et al., 2011). Also shown in Fig. 7 are predicted T_g for various oxygenated compounds originating from the parent structure of *n*-heptadecane (red) and naphthalene (blue). The red-shaded and blue-shaded vertical bars indicate the range of investigated O/C ratio for each SOA. The grey horizontal bar indicates the suggested turnover from liquid behavior at room temperature (no bounce) for substances with a T_g less than ~250 K to solid behavior (bounce) for substances with a T_g above ~270 K.

The predicted T_g of naphthalene is already close to 250 K, and just adding one O-atom (e.g., 1-naphthol and 2-naphthol, with an O/C ratio of 0.1) might initiate (partial) bounce in such particles at room temperature. Further increase in O/C ratio to values between 0.2–0.4 leads to predicted T_g values from close to room temperature up to significantly beyond room temperature, implying full bounce. Even though there is considerable scatter in these data, it is obvious that in the measured range of O/C>0.35 (light blue shading) nearly all substances are expected to bounce independently of their actual O/C ratio.

In contrast, the predicted T_g for *n*-heptadecane and those of mildly oxygenated compounds (1-alcohol, 1-aldehyde, 2-ketone) with an O/C ratio of 0.06 are so low that these compounds are liquid at room temperature and, thus, would not show bounce. Only at significant oxygenation (e.g., the 1,17-dicarboxylic acid, with an O/C ratio of 0.24) bounce is to be expected. We note that oxygenation of *n*-heptadecane is likely to

ACPD
12, 4447–4476, 2012

lead to fragmentation. However, it appears that at least an oxidation to a dicarboxylic acid is required for bounce, more or less independently of the length of the remaining carbon chain (see red open circles with number of C-atoms indicated). Clearly, for *n*-heptadecane T_g passes from ~207 K to greater than ~280 K with increasing O/C in the measured range (pink shading), in agreement with the measurements.

Similar to previous studies that suggest a correlation of bounced fraction with the glass transition temperature (Virtanen et al., 2010) the same correlation is observed here. Based on an idealized comparison of predicted T_g values shown in Fig. 7, it is no surprise that *n*-heptadecane SOA shows a "bounce transition" with increasing O/C in the investigated range while naphthalene SOA bounced at all investigated O/C ratios.

3.4 Discussion

The main factors affecting the bounce behavior of SOA particles are likely their viscosity, elasticity and the surface adhesion. For amorphous particles, the viscosity and mechanical properties are sensitive to the glass transition temperature (Shiraiwa et al., 2011; Koop et al., 2011). The glass transition temperature and thus the viscosity at constant temperature are sensitive to the solvent concentration, molar mass and the functional groups of the particulate matter (Zobrist et al., 2008; Koop et al., 2011). As discussed above, we suggest that humidity-induced changes in bounced fraction of the SOA particle are related to a humidity-induced glass transition of SOA particles (Mikhailov et al., 2009).

The conditions for a humidity-induced glass transition (i.e. liquefaction) are connected to T_g(dry) of the SOA compounds at dry conditions, which is correlated to the inverse molar mass of the compounds. Therefore, we attempt to relate the measured humidity-induced phase transitions of the SOA particles to their molar mass by showing in Fig. 8 the slope of the bounced fraction of SOA particles at RH_f>50 % as a function of precursor inverse molar mass. Measurements in which no phase transitions were observed (e.g. *n*-heptadecane SOA with O/C = 0.10) are not shown in this figure. Markers are colored by the O/C ratio of the SOA. Fig. 8 shows that for SOA particles

ACPD
12, 4447–4476, 2012

produced from isoprene, α-pinene, longifolene, and naphthalene, the "bounce slope" was linearly related to the precursor inverse molar mass. SOA particles produced from *n*-heptadecane did not follow the same trend as the particles generated by the other precursors.

To the extent that the "bounce slope" is proportional to the inverse average molar mass (AMM) of the SOA, Fig. 8 suggests that the AMM of SOA generated from *n*-heptadecane does not scale with precursor AMM in the same way as the SOA in the other experiments. One possible explanation for this observation is that fragmentation reactions that cleave carbon-carbon bonds and lower the AMM are more important in SOA produced from *n*-heptadecane than in the other systems. The importance of fragmentation reactions has not been extensively characterized for precursors studied in this work. However, Chacon-Madrid et al. (2010; 2011) showed that the *OH oxidation of linear aldehydes/ketones formed SOA in lower yields than linear alkanes with equivalent vapor pressures, suggesting that fragmentation is important for SOA generated from alkane precursors. If SOA generated from the other precursors experienced less fragmentation than SOA generated from *n*-heptadecane, this may explain the trends observed in Fig. 8.

4 Conclusions

Our results suggest that most types of atmospherically-relevant SOA form amorphous solid or semi-solid particles at $RH_{/} \lesssim 60\,\%$. These SOA particles can undergo phase transitions as a result of changes in relative humidity, and/or O/C level. Addition of hygroscopic sulphuric acid to the SOA liquefied the mixed particles at low $RH_{/}$, which is consistent with aerosol bounce observations from Virtanen et al. (2011) and T_g measurements from Koop et al. (2011). The phase of the SOA affects corresponding timescales for mass transfer and heterogeneous reactions within the particles (Cappa and Wilson, 2011; Vaden et al., 2011; Shiraiwa et al., 2011), and may influence their ability to serve as cloud condensation nuclei or ice nuclei in the atmosphere.

ACPD
12, 4447–4476, 2012

In most cases, humidity-induced phase changes measured for the SOA were not correlated with O/C ratio or the CCN activity, κ. However, our measurements suggest that humidity-induced phase changes were related to the average molar mass of the SOA. These observations are consistent with the results of Koop et al. (2011), who showed that T_g was more strongly influenced by molar mass than O/C ratio of model organic compounds.

With the exception of SOA produced from *n*-heptadecane, the bounced fraction of SOA particles at RH_f<50 % was insensitive to changes in O/C ratio. The increase in bounced fraction of *n*-heptadecane SOA particles as a function of O/C ratio is consistent with an oxidation-induced phase change from organic liquid particles to organic semi-solid particles. Future work will investigate the prevalence of oxidation-induced phase changes in other types of SOA, as well as the ability of the bounce measurement to provide quantitative measurements of particle viscosity, diffusivity, and glass transition temperature.

Acknowledgements. This work was supported by a grant from the Nessling Foundation to the Tampere University of Technology. The research was also supported by the Office of Science (BER), Department of Energy (Atmospheric Science Program) grant No. DE-SC0006980 and the Atmospheric Chemistry Program of the National Science Foundation grants No. ATM-0525355 and ATM-0854916 to Boston College and Aerodyne Research, Inc, and the EU integrated project 505390-GOCE-CT-2004.

References

Aiken, A. C., DeCarlo, P. F., Kroll, J. H., Worsnop, D. R., Huffman, J. A., Docherty, K. S., Ulbrich, I. M., Mohr, C., Kimmel, J. R., Sueper, D., Sun, Y., Zhang, Q., Trimborn, A., Northway, M., Ziemann, P. J., Canagaratna, M. R., Onasch, T. B., Alfarra, M. R., Prevot, A. S. H., Dommen, J., Duplissy, J., Metzger, A., Baltensperger, U., and Jimenez, J. L.: O/C and OM/OC Ratios of Primary, Secondary, and Ambient Organic Aerosols with High-Resolution Time-of-Flight Aerosol Mass Spectrometry, Environ. Sci. Technol., 42, 4478–4485, doi:10.1021/es703009q, pMID: 18605574, 2008. 4455

Cappa, C. D. and Wilson, K. R.: Evolution of organic aerosol mass spectra upon heating: implications for OA phase and partitioning behavior, Atmos. Chem. Phys., 11, 1895–1911, doi:10.5194/acp-11-1895-2011, 2011. 4450, 4451, 4462

Chacon-Madrid, H. J. and Donahue, N. M.: Fragmentation vs. functionalization: chemical aging and organic aerosol formation, Atmos. Chem. Phys. , 11, 10 553–10 563, doi:10.5194/acp-11-10553-2011, 2011. 4462

Chacon-Madrid, H. J., Presto, A. A., and Donahue, N. M.: Functionalization vs. fragmentation: n-aldehyde oxidation mechanisms and secondary organic aerosol formation, Phys. Chem. Chem. Phys., 12, 13975–13982, doi:10.1039/C0CP00200C, 2010. 4462

DeCarlo, P., Kimmel, J., Trimborn, A., Northway, M., Jayne, J., Aiken, A., Gonin, M., Fuhrer, K., Horvath, T., Docherty, K., Worsnop, D. R., and Jimenez, J. L.: Field-deployable, high-resolution, time-of-flight aerosol mass spectrometer, Analyt. Chem., 78, 8281–8289, 2006. 4455

Donahue, N. M., Kroll, J. H., Pandis, S. N., and Robinson, A. L.: A two-dimensional volatility basis set – Part 2: Diagnostics of organic-aerosol evolution, Atmos. Chem. Phys., 12, 615–634, doi:10.5194/acp-12-615-2012, 2012. 4450

Hallquist, M., Wenger, J. C., Baltensperger, U., Rudich, Y., Simpson, D., Claeys, M., Dommen, J., Donahue, N. M., George, C., Goldstein, A. H., Hamilton, J. F., Herrmann, H., Hoffmann, T., Iinuma, Y., Jang, M., Jenkin, M. E., Jimenez, J. L., Kiendler-Scharr, A., Maenhaut, W., McFiggans, G., Mentel, T. F., Monod, A., Prévôt, A. S. H., Seinfeld, J. H., Surratt, J. D., Szmigielski, R., and Wildt, J.: The formation, properties and impact of secondary organic aerosol: current and emerging issues, Atmospheric Chemistry and Physics, 9, 5155–5236, doi:10.5194/acp-9-5155-2009, 2009. 4449

Höhne, G., Hemminger, W., and Flammersheim, H.: Differential scanning calorimetry, Springer Verlag, 2003. 4458

IPCC: Changes in Atmospheric Constituents and in Radiative Forcing. In: Climate Change 2007: The Physical Science Basis. Contribution of Working Group I to the Fourth Assessment Report of the Intergovernmental Panel on Climate Change, available online at: http://www.ipcc.ch/ipccreports/ar4-wg1.htm, 2007. 4449, 4450

Jimenez, J. L., Canagaratna, M. R., Donahue, N. M., Prevot, A. S. H., Zhang, Q., Kroll, J. H., DeCarlo, P. F., Allan, J. D., Coe, H., Ng, N. L., Aiken, A. C., Docherty, K. S., Ulbrich, I. M., Grieshop, A. P., Robinson, A. L., Duplissy, J., Smith, J. D., Wilson, K. R., Lanz, V. A., Hueglin, C., Sun, Y. L., Tian, J., Laaksonen, A., Raatikainen, T., Rautiainen, J., Vaatto-

ACPD
12, 4447–4476, 2012

vaara, P., Ehn, M., Kulmala, M., Tomlinson, J. M., Collins, D. R., Cubison, M. J., E., Dunlea, J., Huffman, J. A., Onasch, T. B., Alfarra, M. R., Williams, P. I., Bower, K., Kondo, Y., Schneider, J., Drewnick, F., Borrmann, S., Weimer, S., Demerjian, K., Salcedo, D., Cottrell, L., Griffin, R., Takami, A., Miyoshi, T., Hatakeyama, S., Shimono, A., Sun, J. Y., Zhang, Y. M., Dzepina, K., Kimmel, J. R., Sueper, D., Jayne, J. T., Herndon, S. C., Trimborn, A. M., Williams, L. R., Wood, E. C., Middlebrook, A. M., Kolb, C. E., Baltensperger, U., and Worsnop, D. R.: Evolution of Organic Aerosols in the Atmosphere, Science, 326, 1525–1529, doi:10.1126/science.1180353, 2009. 4449, 4457

Kanakidou, M., Seinfeld, J., Pandis, S., Barnes, I., Dentener, F., Facchini, M., Van Dingenen, R., Ervens, B., Nenes, A., Nielsen, C., Swietlicki, E., Putaud, J. P., Balkanski, Y., Fuzzi, S., Horth, J., Moortgat, G. K., Winterhalter, R., Myhre, C. E. L., Tsigaridis, K., Vignati, E., Stephanou, E. G., and Wilson, J.: Organic aerosol and global climate modelling: a review, Atmos. Chem. Phys., 5, 1053–1123, doi:10.5194/acp-5-1053-2005, 2005. 4450

Kirkby, J., Curtius, J., Almeida, J., Dunne, E., Duplissy, J., Ehrhart, S., Franchin, A., Gagné, S., Ickes, L., Kürten, A., Kupc, A., Metzger, A., Riccobono, F., Rondo, L., Schobesberger, S., Tsagkogeorgas, G., Wimmer, D., Amorim, A., F, B., Breitenlechner, M., David, A., Dommen, J., Downard, A., Ehn, M., Flagan, R., Haider, S., Hansel, A., Hauser, D., Jud, W., Junninen, H., Kreissl, F., Kvashin, A., A., L., Lehtipalo, K., Lima, J., Lovejoy, E., Makhmutov, F., Mathot, S., Mikkilä, J., Minginette, P., Mogo, S., Nieminen, T., Onnela, A., Pereira, P., Petäjä, T., Schnitzhofer, R., Seinfeld, S. P., Sipilä, M., Stozhkov, Y., Stratmann, F., Tome, A., Vanhanen, J., Viisanen, Y., Vrtala, A., Wagner, P., Walther, H., Weingartner, E., Wex, H., Winkler, P., Carslaw, K., Worsnop, D., Baltensberger, U., and Kulmala, M.: Role of sulphuric acid, ammonia and galactic cosmic rays in atmospheric aerosol nucleation, Nature, 476, 429–433, 2011. 4459

Koop, T., Bookhold, J., Shiraiwa, M., and Pöschl, U.: Glass transition and phase state of organic compounds: dependency on molecular properties and implications for secondary organic aerosols in the atmosphere, Phys. Chem. Chem. Phys., 13, 19238–19255, doi:10.1039/C1CP22617G, 2011. 4450, 4454, 4457, 4458, 4460, 4461, 4462, 4463

Lambe, A. T., Ahern, A. T., Williams, L. R., Slowik, J. G., Wong, J. P. S., Abbatt, J. P. D., Brune, W. H., Ng, N. L., Wright, J. P., Croasdale, D. R., Worsnop, D. R., Davidovits, P., and Onasch, T. B.: Characterization of aerosol photooxidation flow reactors: heterogeneous oxidation, secondary organic aerosol formation and cloud condensation nuclei activity measurements, Atmos. Meas. Tech., 4, 445–461, doi:10.5194/amt-4-445-2011, 2011. 4452, 4455

ACPD
12, 4447–4476, 2012

Lance, S., Nenes, A., Medina, J., and Smith, J. N.: Mapping the Operation of the DMT Continuous Flow CCN Counter, Aerosol Science and Technology, 40, 242–254, doi:10.1080/02786820500543290, 2006. 4455

Mao, J., Ren, X., Brune, W. H., Olson, J. R., Crawford, J. H., Fried, A., Huey, L. G., Cohen, R. C., Heikes, B., Singh, H. B., Blake, D. R., Sachse, G. W., Diskin, G. S., Hall, S. R., and Shetter, R. E.: Airborne measurement of OH reactivity during INTEX-B, Atmos. Chem. Phys., 9, 163–173, doi:10.5194/acp-9-163-2009, 2009. 4453

Massoli, P., Lambe, A., Ahern, A., Williams, L., Ehn, M., Mikkilä, J., Canagaratna, M., Brune, W., Onasch, T., Jayne, J., Petäjä, T., Kulmala, M., A., L., Kolb, C. E., Davidovits, P., and Worsnop, D.: Relationship between aerosol oxidation level and hygroscopic properties of laboratory generated secondary organic aerosol (SOA) particles, Geophys. Res. Lett, 37, L24801, doi:10.1029/2010GL045258, 2010. 4455

Mikhailov, E., Vlasenko, S., Martin, S., Koop, T., and Pöschl, U.: Amorphous and crystalline aerosol particles interacting with water vapor: conceptual framework and experimental evidence for restructuring, phase transitions and kinetic limitations, Atmos. Chem. Phys., 9, 9491–9522, doi:10.5194/acp-9-9491-2009, 2009. 4450, 4461

Murray, B. J.: Inhibition of ice crystallisation in highly viscous aqueous organic acid droplets, Atmos. Chem. Phys., 8, 5423–5433, doi:10.5194/acp-8-5423-2008, 2008. 4450

Pankow, J.: An absorption model of the gas/aerosol partitioning involved in the formation of secondary organic aerosol, Atmos. Environ.,, 28, 189–193, doi:10.1016/1352-2310(94)90094-9, 1994. 4450

Pedernera, D. A.: Glass formation in upper tropospheric aerosol particles (in German), Ph.D. thesis, Bielefeld University, available online at: http://pub.uni-bielefeld.de/publication/2303351, 2008. 4473

Petters, M. D. and Kreidenweis, S. M.: A single parameter representation of hygroscopic growth and cloud condensation nucleus activity, Atmos. Chem. Phys., 7, 1961–1971, doi:10.5194/acp-7-1961-2007, 2007. 4455

Pfrang, C., Shiraiwa, M., and Pöschl, U.: Chemical ageing and transformation of diffusivity in semi-solid multi-component organic aerosol particles, Atmos. Chem. Phys., 11, 7343–7354, doi:10.5194/acp-11-7343-2011, 2011. 4450

Roberts, G. and Nenes, A.: A continuous-flow streamwise thermal-gradient CCN chamber for atmospheric measurements, Aerosol Sci. Technol., 39, 206–221, 2005. 4455

Saukko, E., Kuuluvainen, H., and Virtanen, A.: A method to resolve the phase state of aerosol

ACPD
12, 4447–4476, 2012

particles, Atmos. Meas. Tech., 5, 259–265, doi:10.5194/amt-5-259-2012, 2012. 4453, 4454
Seinfeld, J. and Pandis, S.: Atmospheric chemistry and physics: from air pollution to climate change, Wiley, New York, USA, 2nd edn., 1998. 4453
Shiraiwa, M., Ammann, M., Koop, T., and Pöschl, U.: Gas uptake and chemical aging of semisolid organic aerosol particles, Proc. Natl. Acad. Sci., 108, 11003–11008, doi:10.1073/pnas.1103045108, 2011. 4450, 4461, 4462
Sipilä, M., Berndt, T., Petäjä, T., Brus, D., Vanhanen, J., Stratmann, F., Patokoski, J., Mauldin, R. L., Hyvärinen, A.-P., Lihavainen, H., and Kulmala, M.: The Role of Sulfuric Acid in Atmospheric Nucleation, Science, 327, 1243–1246, doi:10.1126/science.1180315, 2010. 4459
Vaden, T. D., Imre, D., Beránek, J., Shrivastava, M., and Zelenyuk, A.: Evaporation kinetics and phase of laboratory and ambient secondary organic aerosol, Proceedings of the National Academy of Sciences, 108, 2190–2195, doi:10.1073/pnas.1013391108, 2011. 4450, 4451, 4462
Virtanen, A., Joutsensaari, J., Koop, T., Kannosto, J., Yli-Pirilä, P., Leskinen, J., Mäkelä, J., Holopainen, J., Pöschl, U., Kulmala, M., Worsnop, D. R., and Laaksonen, A.: An amorphous solid state of biogenic secondary organic aerosol particles, Nature, 467, 824–827, 2010. 4450, 4451, 4459, 4461
Virtanen, A., Kannosto, J., Kuuluvainen, H., Arffman, A., Joutsensaari, J., Saukko, E., Hao, L., Yli-Pirilä, P., Tiitta, P., Holopainen, J. K., Keskinen, J., Worsnop, D. R., Smith, J. N., and Laaksonen, A.: Bounce behavior of freshly nucleated biogenic secondary organic aerosol particles, Atmos. Chem. Phys., 11, 8759–8766, doi:10.5194/acp-11-8759-2011, 2011. 4459, 4462
Zahardis, J. and Petrucci, G. A.: The oleic acid-ozone heterogeneous reaction system: products, kinetics, secondary chemistry, and atmospheric implications of a model system – a review, Atmos. Chem. Phys., 7, 1237–1274, doi:10.5194/acp-7-1237-2007, 2007. 4450
Zobrist, B., Marcolli, C., Pedernera, D. A., and Koop, T.: Do atmospheric aerosols form glasses?, Atmos. Chem. Phys., 8, 5221–5244, doi:10.5194/acp-8-5221-2008, 2008. 4450, 4458, 4461
Zobrist, B., Soonsin, V., Luo, B. P., Krieger, U. K., Marcolli, C., Peter, T., and Koop, T.: Ultra-slow water diffusion in aqueous sucrose glasses, Phys. Chem. Chem. Phys., 13, 3514–3526, doi:10.1039/C0CP01273D, 2011. 4454

ACPD
12, 4447–4476, 2012

Table 1. SOA generation parameters and measurements. The third α-pinene line with *OH exposure of 0 refers to an ozonolysis experiment.

Precursor(s)	*OH exposure (10^{11} molec×cm^{-3}s)	O/C	H/C	κ
Isoprene	22.0	0.62	1.7	0.21
Isoprene	7.82	0.61	1.75	0.15
α-pinene	15.5	0.69	1.36	0.19
α-pinene	11.4	0.55	1.45	0.17
α-pinene	0	0.34	1.52	0.14
Longifolene	22.0	0.58	1.31	0.19
Longifolene	2.77	0.14	1.53	0.05
Longifolene+SO_2	22.0	0.55	1.77	0.19
Longifolene+SO_2	22.0	0.57	1.74	0.17
Longifolene+SO_2	22.0	0.75	1.49	0.21
Naphthalene	22.0	1.41	0.90	0.18
Naphthalene	7.82	0.68	0.97	0.15
Naphthalene	2.77	0.35	0.92	0.16
n-heptadecane	11.4	0.30	1.69	0.12
n-heptadecane	7.82	0.20	1.78	0.11
n-heptadecane	4.95	0.15	1.85	0.04
n-heptadecane	2.77	0.10	1.92	0.01

ACPD
12, 4447–4476, 2012

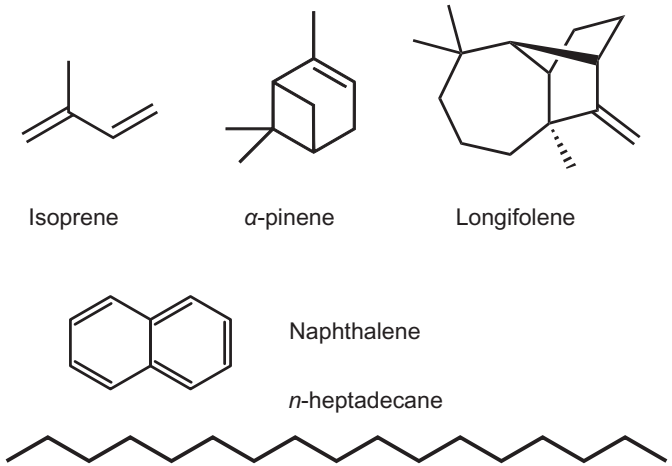

Fig. 1. Molecular structures of the VOC and IVOC gaseous precursors used to generate SOA for the experiment: biogenic precursors are in the top row, anthropogenic model precursors are on the bottom.

ACPD
12, 4447–4476, 2012

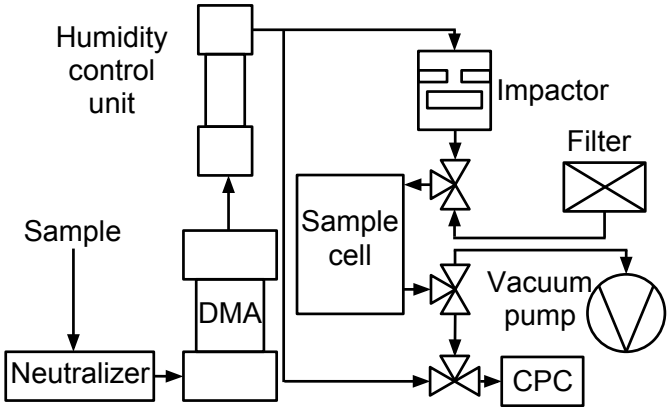

Fig. 2. The measurement system for the particle phase measurement.

ACPD
12, 4447–4476, 2012

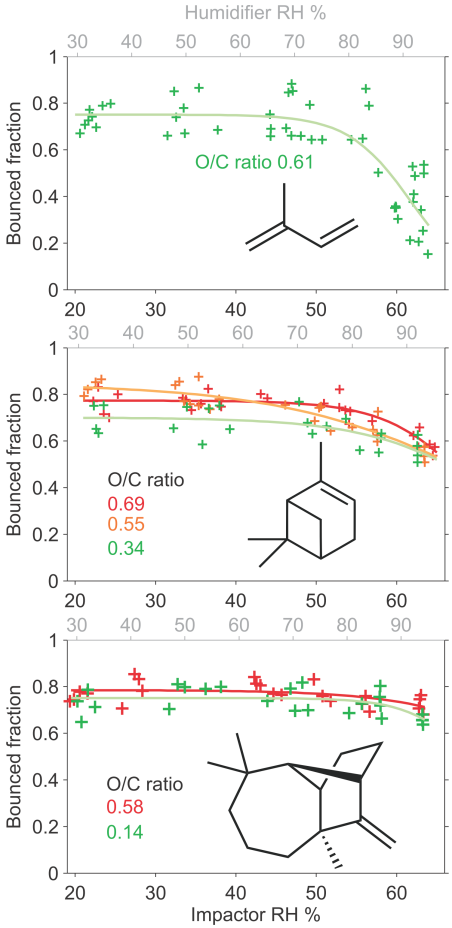

Fig. 3. Bounce behavior of SOA from photo-oxidation experiments of biogenic precursors, solid lines are sigmoid fits to guide the eye. Upper panel: isoprene SOA, middle panel: α-pinene SOA, lower panel: longifolene SOA.

ACPD
12, 4447–4476, 2012

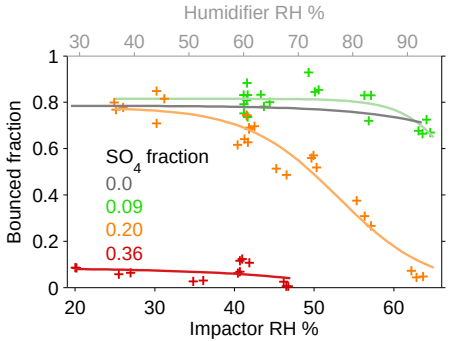

Fig. 4. Addition of SO_2 to precursor flow decreases the phase transition relative humidity. SO_4 fraction indicates the measured fraction of SO_4 of the total mass (including organic carbon compounds, ammonia and SO_4) of the particles.

ACPD
12, 4447–4476, 2012

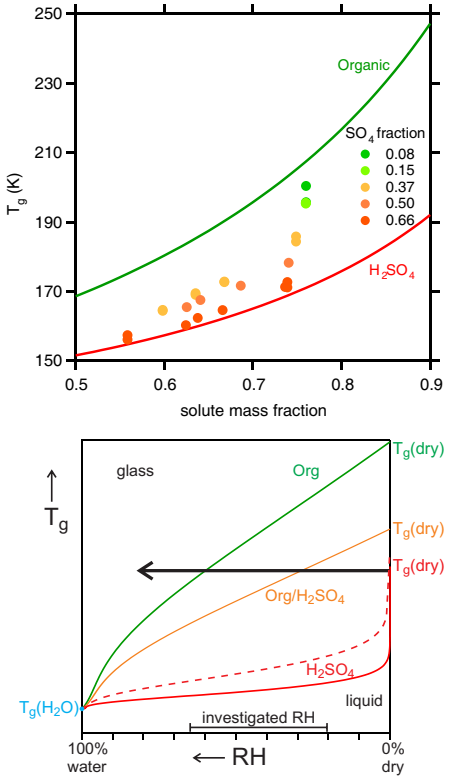

Fig. 5. Top: Addition of H_2SO_4 to an organic (here: glucose) leads to a strong reduction in T_g at the same water content (Pedernera, 2008). The effect is even more pronounced when plotted as a function of relative humidity (because of the different hygroscopicities of organics and sulfate). The bottom panel is a schematic picture of T_g versus equilibrium relative humidity for various organic/sulphuric acid mixtures.

ACPD
12, 4447–4476, 2012

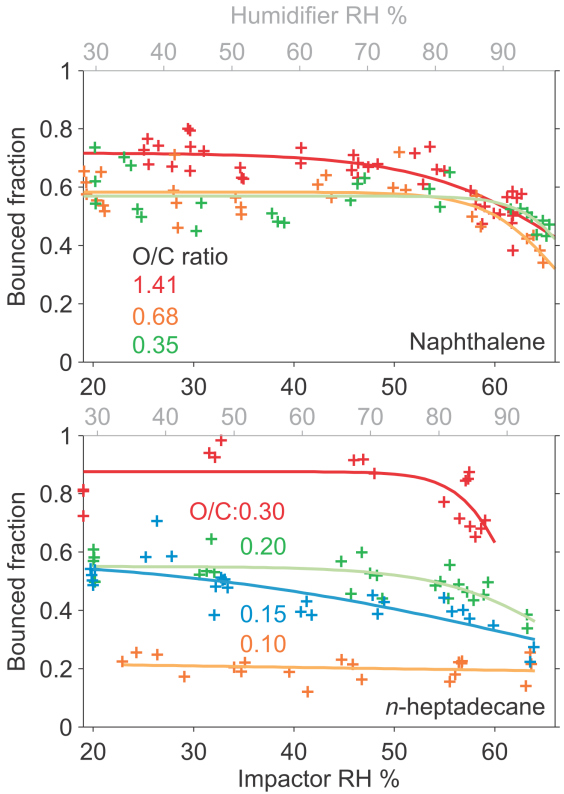

Fig. 6. Bounce behavior of SOA from photo-oxidation of naphthalene (upper panel) and *n*-heptadecane (lower panel).

ACPD
12, 4447–4476, 2012

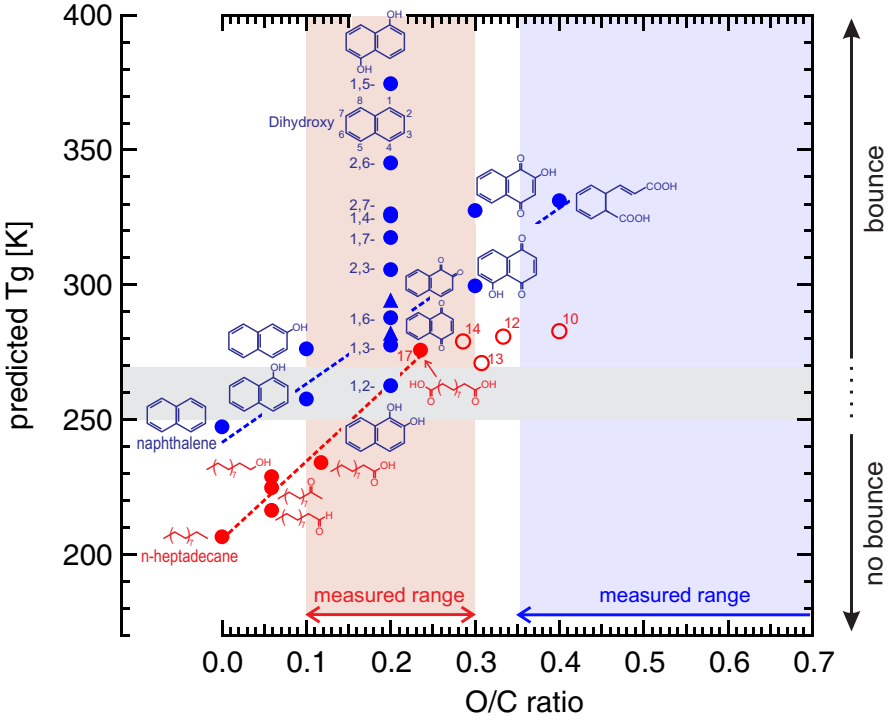

Fig. 7. Predicted glass transition temperatures T_g as a function of the molecular O/C ratio for various oxygenated compounds originating from the parent structure of *n*-heptadecane (red) and naphthalene (blue). Open circles are predicted T_g for *n*-dicarboxylic acids with the number of C-atoms indicates for each point. For details see text.

ACPD
12, 4447–4476, 2012

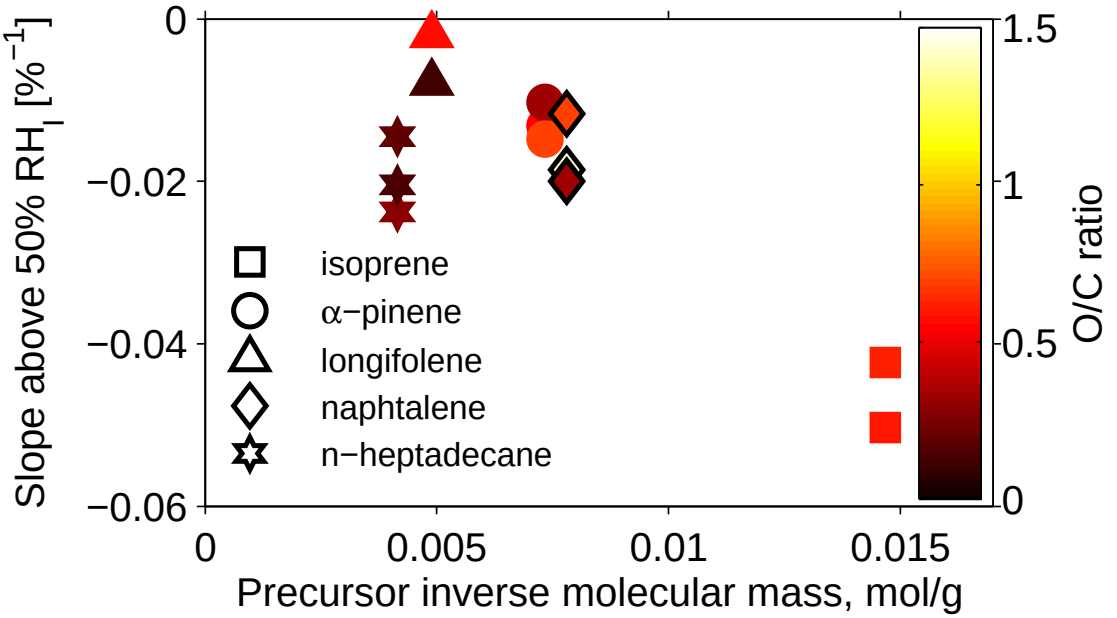

Fig. 8. The slope of the bounce at RH$_l$>50 % versus precursor inverse molar mass for the studied systems.

ACPD
12, 4447–4476, 2012